iScience

CellPress
OPEN ACCESS

Article

Newcastle-disease-virus-induced ferroptosis through nutrient deprivation and ferritinophagy in tumor cells

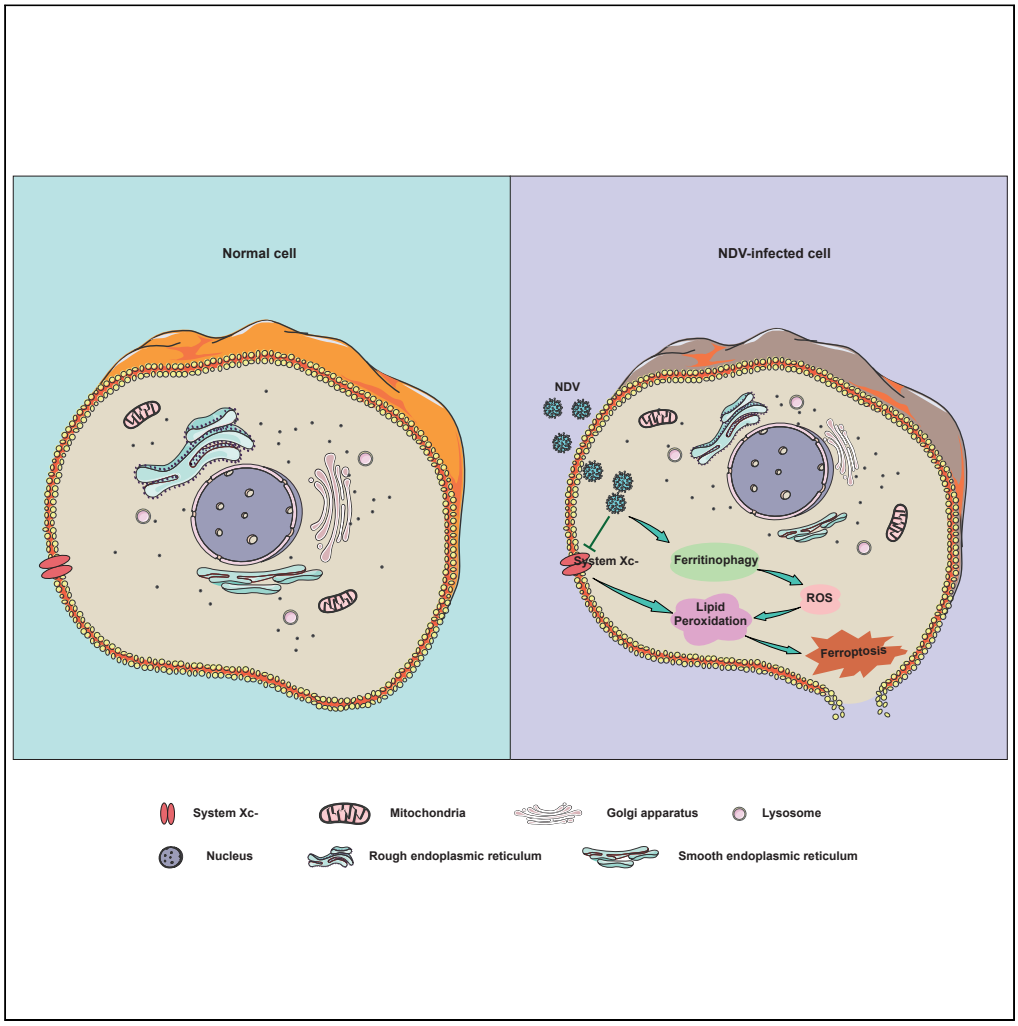

Xianjin Kan, Yuncong Yin, Cuiping Song, ..., Songshu Meng, Yingjie Sun, Chan Ding

shoveldeen@shvri.ac.cn (C.D.)
sunyingjie@shvri.ac.cn (Y.S.)

Highlights

Oncolytic viruses NDV caused tumor cells death through ferroptosis

NDV-induced ferroptosis acts through nutrient deprivation by suppression of System Xc^-

P53 activation is required for NDV-induced ferroptosis initiation

Ferritinophagy induced by NDV promotes ferroptosis through release of ferrous iron

Kan et al., iScience *24*, 102837
August 20, 2021
https://doi.org/10.1016/j.isci.2021.102837

iScience

CellPress
OPEN ACCESS

Article

Newcastle-disease-virus-induced ferroptosis through nutrient deprivation and ferritinophagy in tumor cells

Xianjin Kan,[1,4] Yuncong Yin,[2,4] Cuiping Song,[1] Lei Tan,[1] Xusheng Qiu,[1] Ying Liao,[1] Weiwei Liu,[1] Songshu Meng,[3] Yingjie Sun,[1,5,*] and Chan Ding[1,2,5,6,*]

SUMMARY

A number of new cell death processes have been discovered in recent years, including ferroptosis, which is characterized by the accumulation of lipid peroxidation products derived from iron metabolism. The evidence suggests that ferroptosis has a tumor-suppressor function. However, the mechanism by which ferroptosis mediates the response of tumor cells to oncolytic viruses remains poorly understood. The Newcastle disease virus (NDV) can selectively replicate in tumor cells. We show that NDV-induced ferroptosis acts through p53-SLC7A11-GPX4 pathway. Meanwhile, the levels of intracellular reactive oxygen species and lipid peroxides increased in tumor cells. Ferritinophagy was induced by NDV promotion of ferroptosis through the release of ferrous iron and an enhanced Fenton reaction. Collectively, these observations demonstrated that the NDV can kill tumor cells through ferroptosis. Our study provides novel insights into the mechanisms of NDV-induced ferroptosis and highlights the critical role of viruses in treating therapy-resistant cancers.

INTRODUCTION

Ferroptosis, a newly discovered form of regulated cell death, involves iron and reactive oxygen species (ROS), and is characterized by the accumulation of phospholipid peroxides (Chu et al., 2019; Dixon et al., 2012; Doll et al., 2017; Jiang et al., 2015; Tang et al., 2021; Yang et al., 2014). The peroxidation of phospholipids and the accumulation of lipid ROS are the key drivers of ferroptosis-induced cell death (Su et al., 2019; Ubellacker et al., 2020). Ferroptosis is initiated through various pathways, including the depletion of intracellular glutathione (GSH) and lipid peroxidation, caused by increases in oxidizing iron and the labile iron pool (Cao and Dixon, 2016; Gao et al., 2019; Hadian and Stockwell, 2020; Muri et al., 2019). GSH is an antioxidant tripeptide consisting of glutamate, cysteine, and glycine (Lv et al., 2019). Recent studies have reported that GSH acts as important regulator of cellular antioxidant defenses. The depletion of cystine and/or GSH results in the iron-dependent accumulation of lethal lipid ROS, which is accompanied by ferroptosis. This process is suppressed by lipophilic antioxidants such as ferrostatin-1 (Dixon and Stockwell, 2014; Hassannia et al., 2019). In contrast, GSH depletion results in the inactivation of GSH-dependent peroxidase 4 (GPX4), a member of the GSH oxidoreductases (GPXs) family, which directly reduces lipid peroxides (Alborzinia et al., 2018). Recent studies have shown that ferroptosis is initiated by the direct depletion or indirect inhibition of coenzyme Q10 via the squalene synthase mevalonate pathway (Bersuker et al., 2019; Doll et al., 2019; Stockwell et al., 2017).

System X_C^-, a cystine/glutamate antiporter, consists of SLC7A11and SLC3A2 and is responsible for maintaining redox homeostasis by importing cystine for the synthesis of the major antioxidant GSH (Xie et al., 2016). Recent investigations have shown that p53 plays a role in the regulation of ferroptosis processes (Jiang et al., 2015; Tarangelo et al., 2018; Wang et al., 2016c; Xie et al., 2017). p53-induced ferroptosis is responsible for tumor suppression through system X_C^-, and acetylation is crucial for p53-mediated ferroptosis (Wang et al., 2016c). The function of SLC7A11 is also affected by nuclear-factor-erythroid 2-related factor 2 (NRF2) and beclin 1 (BECN1). NRF2 upregulates SLC7A11 expression, thereby preventing ferroptosis-mediated cell death (Anandhan et al., 2020; Sun et al., 2016; Yu et al., 2020). BECN1 inhibits system X_C^- activity by binding directly to SLC7A11 (Song et al., 2018). Ferritinophagy is a selective form

[1]Department of Avian Infectious Diseases, Shanghai Veterinary Research Institute. Chinese Academy of Agricultural Science, Shanghai 200241, P.R. China

[2]College of Veterinary Medicine, Yangzhou University, Yangzhou 225009, Jiangsu Province, China

[3]Institute of Cancer Stem Cell, Dalian Medical University, Dalian 116044, PR China

[4]These authors contributed equally

[5]These authors contributed equally

[6]Lead contact

*Correspondence: shoveldeen@shvri.ac.cn (C.D.), sunyingjie@shvri.ac.cn (Y.S.)

https://doi.org/10.1016/j.isci.2021.102837

of autophagy that contributes to the initiation of ferroptosis through the degradation of ferritin by lysosomes (Qin et al., 2021; Zhou et al., 2020). Nuclear receptor coactivator 4 (NCOA4), a selective cargo receptor, promotes ferritin degradation during ferritinophagy (Goodall and Thorburn, 2014; Ito et al., 2021; Nai et al., 2021). The accumulation of ferrous iron triggers ROS generation through the Fenton reaction, and ferritinophagy modulates ferroptosis by increasing the levels of lipid peroxidation (Ajoolabady et al., 2021). Ferritin deficiency also induces ferroptosis through the downregulation of SLC7A11, suggesting that the ferritin-SLC7A11-GSH axis plays an important role in the initiation of ferroptosis (Fang et al., 2020).

In recent years, there has been renewed interest in ferroptosis in cancer cells (Angeli et al., 2017; Wang et al., 2016a; Yang and Stockwell, 2016; Zhou et al., 2020). The Newcastle disease virus (NDV) is a paramyxovirus that infects large poultry populations, and the NDV has been investigated as an oncolytic agent because it replicates selectively in tumor cells (Alexander, 2000; Fiola et al., 2006; Mansour et al., 2011). Many recent studies have shown that NDV promotes oncolytic activity and induces tumor cell death through the caspase-dependent pathway or activates ataxia telangiectasia-mutated (ATM) kinase-mediated double-strand break signals (Li et al., 2019; Ren et al., 2020). However, there are currently no reports showing whether the oncolytic virus kills tumor cells through ferroptosis. Here, we showed that oncolytic NDV kills cancer cells through ferroptosis via upregulation of p53 expression and suppression of system X_C^-, resulting in the reduction of GPX4 activity. Our study identifies a novel mechanism of oncolytic-virus-induced cell death, and the regulation of ferroptosis may be a promising new way to increase the oncolytic effect of therapies, especially for those therapy-resistant cancers.

RESULTS

NDV induces cell death through ferroptosis

Many studies have demonstrated that oncolytic viruses kill cancer cells via various pathways, including apoptosis, autophagy, and pyroptosis (Colunga et al., 2010; Fiola et al., 2006; Koks et al., 2015). However, the role of ferroptosis in oncolytic-virus-induced cell death has not been investigated. Here, we first evaluated whether the NDV induces ferroptosis in U251 glioma cells. Erastin, the ferroptosis inducer, which inhibits system X_C^- and prevents cystine import, and RSL3, which inhibits GPX4 directly, were used as the positive controls (Dixon et al., 2012). The morphology of cell death caused by NDV strain Herts/33 was in consistent with ferroptosis inducer treatment determined under the microscope. Different from other cell death, NDV-infection-induced cell death showed no nucleus rupture and wrinkle (Figure 1A). Cell death was quantified by assaying lactate dehydrogenase release using a cytotoxic detection kit. Consistently, cell viability decreased significantly upon NDV infection and treatment with the ferroptosis inducer compared with that in control cells (Figure 1B). The occurrence of free iron in living cells has recently attracted attention because its high reactivity may be related to cell damage or death (Dixon et al., 2012). Ferroptosis initiation depends on the availability of ferrous iron (Fe^{2+}) (Hassannia et al., 2019; Masaldan et al., 2018), so we examined whether NDV infection increased the level of intercellular ferrous iron. As expected, the NDV increased ferrous iron levels in living cells, which were detected with fluorescent probes (Figures 1C and 1D). Cellular ROS are derived from superoxide radicals, which damage the membranes of cells and organelles (Dixon and Stockwell, 2014; Hassannia et al., 2019). An increased prevalence of ROS was observed in NDV-infected and ferroptosis-inducer-treated cells compared with that in the control groups (Figures 1E and 1F). Accordingly, the oxidative stress marker malondialdehyde (MDA) increased after NDV infection (Figure 1G). Meanwhile, an increase in lipid peroxidation was confirmed by fluorescence observations using Liperfluo (Green) (Figures 1H and 1I). ZJ1, a different strain of the NDV, also induced the substantial upregulation of lipid peroxide and Fe^{2+} levels, further confirming the ferroptosis induced by NDV (S1A-D).

Having shown that oncolytic NDV-induced cell death through ferroptosis, we next tested whether ferroptosis inhibitor blocked U251 cell death in oncolytic NDV-infected cells. Liproxstain-1, a specialized ferroptosis inhibitor, prevents ROS accumulation and cell death in $GPX4^{-/-}$ cells (Xie et al., 2016). Our results showed that cell death was rescued in liproxstain-1-treated NDV-infected cells to some extent (Figure 1J), and that levels of MDA were significantly reduced compared with those in cells only infected with the NDV (Figure 1K). The expression level of lipid peroxides was significantly downregulated in liproxstain-1-treated cells upon NDV infection (S1E and 1F). Collectively, these results showed that NDV-induced cell death through ferroptosis, and the cell death ratio, can be rescued by a ferroptosis inhibitor.

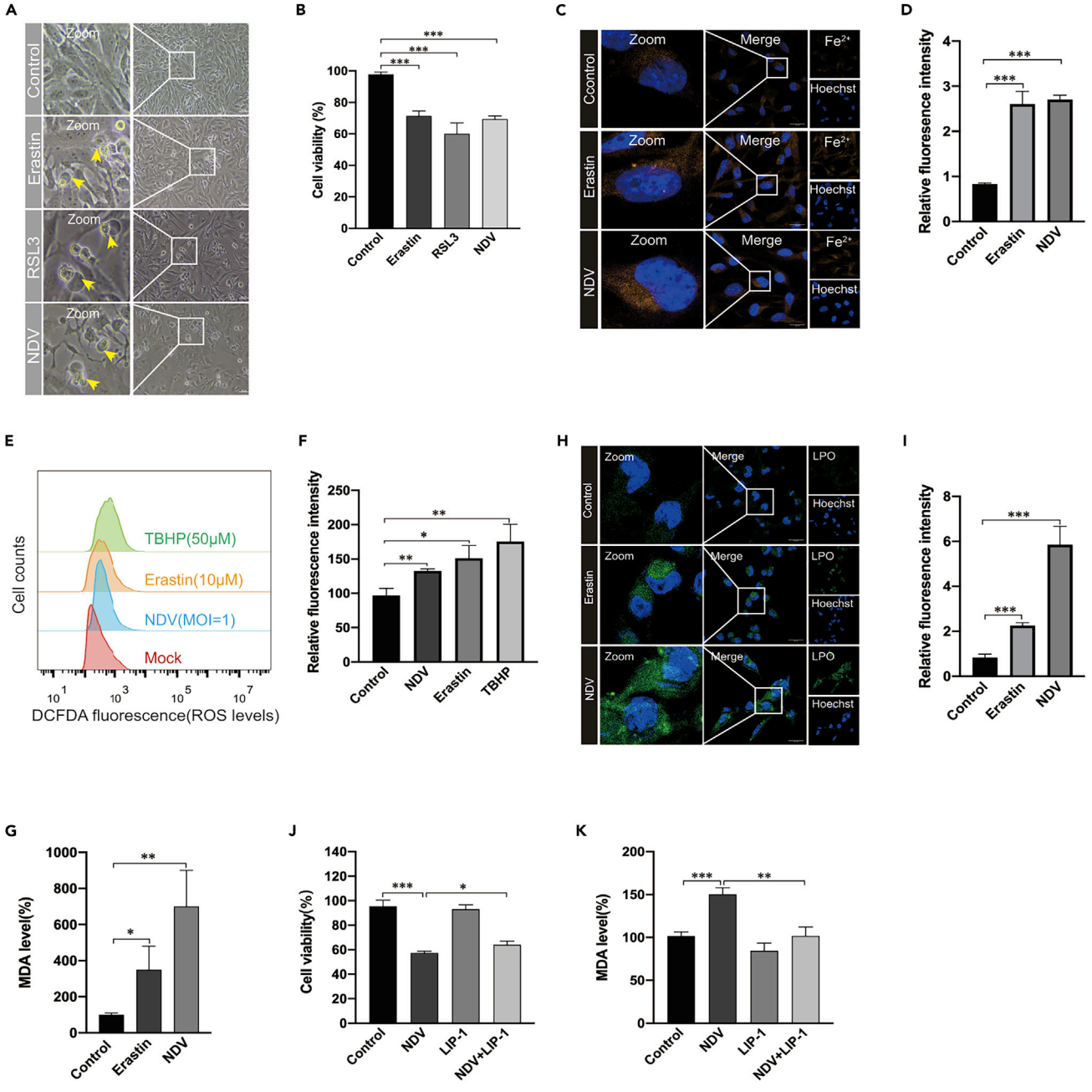

Figure 1. NDV induces cell death through ferroptosis

(A) U251 cells were treated with erastin (5 μM), RSL3 (3 μM), and NDV (MOI = 1) for 24 h, when the images were taken. Scale bars = 200 μm.

(B) Relative levels of cell viability were assayed by measuring LDH release.

(C and D) Analysis of Fe^{2+} levels in U251 cells after erastin (5 μM) treatment for 24 h using the fluorescent probe FerroOrange (Orange). Scale bars = 20 μm.

(E and F) Analysis of intracellular ROS levels using DCFDA staining, and flow cytometry of U251 cells treated for 24 h with the compounds indicated. TBHP (50 μM) was used as the positive control.

(H and I) Intracellular LPO in U251 cells treated with or without erastin (5 μM) and NDV (MOI = 1) for 24 h were determined with the fluorescent probe Liperfluo (Green). Scale bars = 20 μm.

(G) Detection of MDA concentrations in cell lysates was according to the instructions of the kit manufacturer.

(J) Cell death was examined with an LDH assay after 24 h of pretreatment with Liproxstain-1.

(K) Detection of MDA concentration in cell lysates after 24 h of pretreatment with Liproxstain-1.

Significance was analyzed using a two-tailed Student's t-test. *$p < 0.05$; **$p < 0.01$; ***$p < 0.001$. Data were expressed as mean ± SEM (n = 3 in each group).

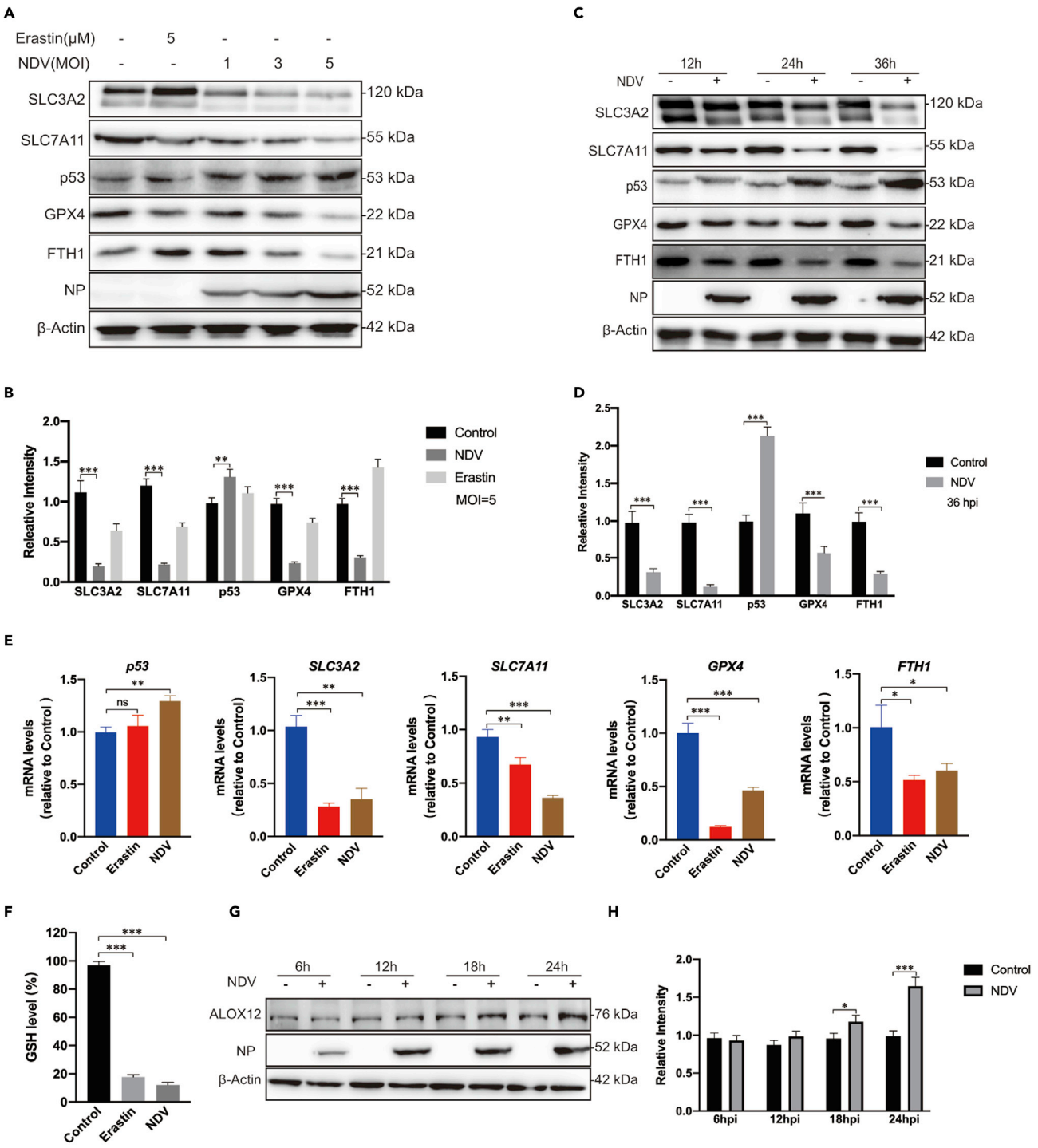

Figure 2. NDV induces ferroptosis by suppressing system X_C^- and activating p53

(A and B) Cell lysates were analyzed for the levels of p53, SLC7A11, SLC3A2, GPX4, FTH1 and NP, in an MOI dependent manner by Western blot. β-actin was used as the loading control. Erastin (5 μM) was added as a ferroptosis inducer.

(C and D) Western blot analyses of the levels of p53, SLC7A11, SLC3A2, GPX4, NP, and FTH1 in U251 cells, with timepoints indicated. β-actin was served as a loading control.

(E) mRNA levels of p53, SLC7A11, SLC3A2, FTH1, and GPX4 in U251 cells treated with NDV (MOI = 1).

Figure 2. *Continued*

(F) Detection of intracellular GSH concentration after NDV infection.

(G and H) Cell lysates were analyzed for the levels of ALOX12 and NP in a time-dependent manner with western blotting. β-actin was included as the loading control.

Significance was analyzed using a two-tailed Student's t-test. *$p < 0.05$; **$p < 0.01$; ***$p < 0.001$. Data were expressed as mean ± SEM (n = 3 in each group).

NDV enables ferroptosis through the suppressor system Xc^- by activating p53

To determine the mechanism of NDV-induced ferroptosis, we examined whether NDV actives ferroptosis by directly blocking system X_C^-. Consistent with previous studies showing that erastin induces ferroptosis by directly targeting system X_C^-, our results suggest that NDV strain Herts/33 suppresses the expression of SLC7A11 and SLC3A2 in a dose- and time-dependent manner (Figures 2A–2D). Activation of p53, a tumor suppressor gene, is known to be required for ferroptosis in cancer cells. Previous studies showed that SLC7A11 protein levels and SLC7A11 mRNA expression are negatively regulated by p53 (Jiang et al., 2015). As expected, our results indicated that NDV also upregulated protein and mRNA levels of p53, accompanied by the downregulation of the protein and mRNA levels of SLC7A11 (Figures 2A–2E). Remarkably, compared with the control group, the reduced GSH levels decreased 5.5- and 8.2-fold in response to erastin treatment and NDV infection, respectively, as measured using a GSSG/GSH quantification kit (Figure 2F). Accordingly, noticeable time- and dose-dependent reductions in the protein and mRNA levels of GPX4 were observed (Figures 2A–2E). Recent studies have shown that 12-lipoxygenase (ALOX12) is required for p53-mediated tumor suppression through a distinct ferroptosis pathway (Chu et al., 2019). Consistent with the results of Chu et al., ALOX12 increased in a time-dependent manner in NDV-infected U251 cells (Figures 2G and 2F). NDV strain ZJ1 was used for further confirmation. The results showed that ZJ1 upregulated the expression of p53 and meanwhile downregulated that of SLC7A11, SLC3A2 and GPX4 (S1G and 1H). Taken together, the results presented confirm that the system X_C^-–GSH–GPX4 axis is inhibited in response to NDV infection. p53 is probably involved in NDV-induced ferroptosis via the inhibition of the system X_C^-.

p53 plays a positive role in NDV-induced ferroptosis

Given that p53 accumulated significantly after NDV infection, accompanied by the inhibition of the system X_C^-–GSH–GPX4 axis, next we investigated the role of p53 in NDV-induced ferroptosis. PFTα HBr (5 μM), a p53 inhibitor, did not affect SLC7A11 and GPX4 protein levels in non-NDV-infected cells, but rescued the protein levels of SLC7A11 and GPX4 in NDV-infected cells (Figures 3A and 3B). We next tested whether PFTα affected MDA production and GSH depletion. Compared with the control group, MDA production was decreased (Figure 3C) and GSH was rescued after cotreatment with PFTα in NDV-infected cells (Figure 3D). Moreover, cell death was rescued in PFTα treated NDV-infected cells (S1I). In accordance with this, lipid peroxide fluorescent intensity was significantly inhibited by PFTα in NDV-infected cells (Figures 3E and 3F). To confirm the intrinsic role of p53 in ferroptosis caused by NDV, small interfering RNA knockdown experiments were performed. As expected, p53 knockdown also rescued the protein levels of SLC7A11 and GPX4 in NDV-infected cells (Figures 3G, 3H, and S1J). We then examined the mRNA expression levels of SLC7A11 and GPX4. Our investigation showed that p53 knockdown significantly upregulated the mRNA expression level of SLC7A11 but not GPX4 (S1K). To further illustrate the ways in which p53 plays an important role in NDV-induced ferroptosis, we examined role of p53 in the formation of ROS. As expected, ROS levels were significantly reduced when NDV-infected cells were treated with PFTα (Figures 3I and 3J). Collectively, our inhibitor and knockdown experiments demonstrate that p53 plays a positive role in NDV-induced ferroptosis.

Ferritinophagy induced by theNDV contributes to ferroptosis initiation

Ferritinophagy, a new type of autophagy, is characterized by the degradation of ferritin, which promotes ferroptosis through autophagy. Nuclear receptor coactivator 4 (NCOA4), a selective cargo receptor, is involved in the autophagic turnover of ferritin in ferroptosis (Goodall and Thorburn, 2014; Hou et al., 2016). Therefore, we first established whether NDV can induce ferritinophagy in U251 cells. Western blot results showed that NCOA4 levels were significantly reduced in NDV-infected cells and that the expression viral NP proteins were inhibited by the autophagy inhibitor, bafilomycin A (BafA1, an H-ATPase inhibitor). Also, NCOA4 degradation was recovered after treatment of Baf-A1 in a dose-dependent manner (Figure 4A). Next, we determined the LC3-II lipidation levels in NDV-infected cells. LC3 lipidation significantly increased in NDV-infected cells treated with bafilomycin A (Figure 4A). Confocal microscopy was used to detect the formation of autophagosomes, seen as green dots. U251 cells were infected with a lentiviral vector encoding a GFP-LC3 reporter. U251 cells stably expressing GFP-LC3 can be used to identify

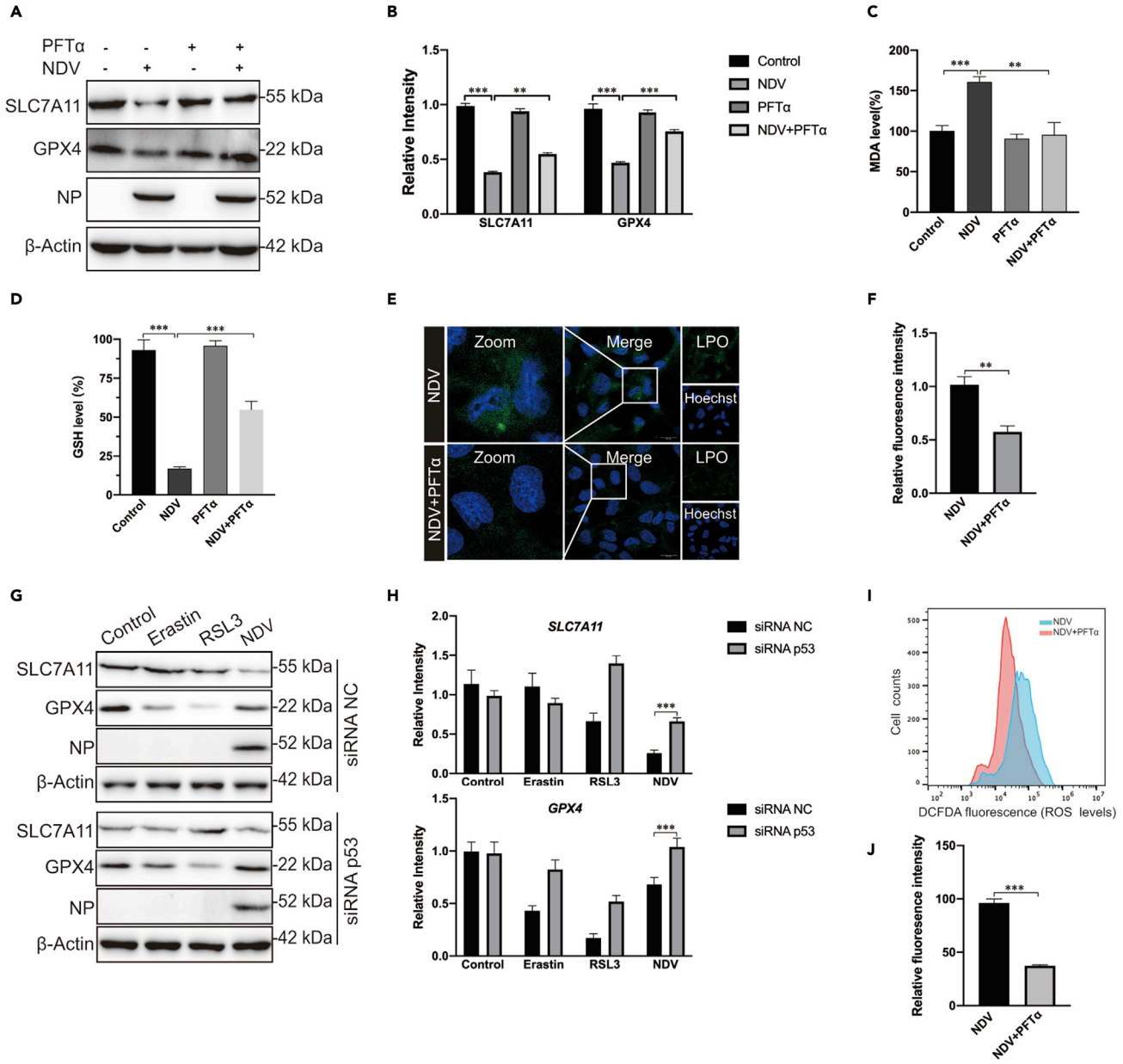

Figure 3. p53 positively regulated ferroptosis caused by NDV

(A and B) Western blotting analysis of the levels of SLC7A11, GPX4, and NP after PFTα (5 μM) treatment for 24 h in NDV-infected U251 cells. β-actin was used as the loading control.

(C) Relative levels of intercellular MDA were assayed after 24 h of pretreatment with PFTα (5 μM) in U251 cells.

(D) Detection of intracellular GSH concentrations for 24 h after pretreatment with PFTα (5 μM) in U251 cells.

(E and F) Intracellular LPO in NDV-infected U251 cells treated with or without PFTα for 24 h was determined with the fluorescent probe Liperfluo (Green). Scale bars = 20 μm.

(G and H) U251 cells with stable knockdown of p53 were treated with erastin (5 μM), RSL3 (5 μM), and NDV (MOI = 5) for 24 h. Western blotting analyses were performed to determine the levels of SLC7A11, GPX4, and NP.

(I and J) Analysis of intracellular ROS levels using DCFDA staining and flow cytometry in U251 cells treated for 24 h with PFTα (5 μM).

Significance was analyzed using a two-tailed Student's t-test. *$p < 0.05$; **$p < 0.01$; ***$p < 0.001$. Data were expressed as mean ± SEM (n = 3 in each group).

autophagosomes. Our studies showed that NDV significantly increased the number of green dots compared with the control group, and the autolysosomes colocalized with the lysosomes (Fig. S2A). We then examined whether the cargo receptor NCOA4 colocalized with autolysosomes (Figure 4B). Excess

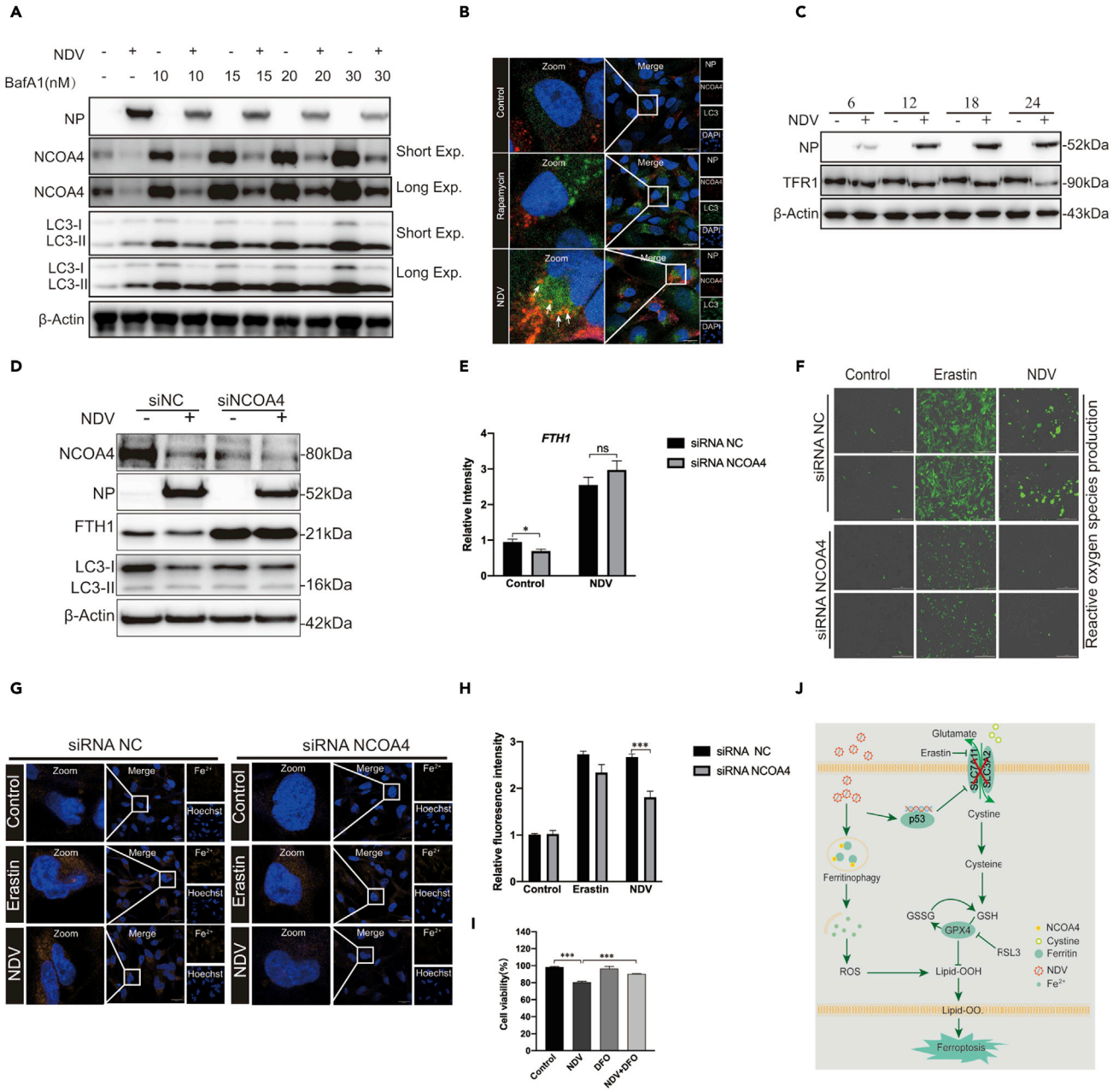

Figure 4. Ferritinophagy induced by NDV contributes to ferroptosis initiation

(A) Western blot analysis of the levels of LC3 and NCOA4 in NDV-infected U251 cells. Baf-A1 was used as an autophagy inhibitor. β-actin was used as the loading control.

(B) Fluorescence microscopy was used to colocalize NCOA4 (red) and LC3 (green) in U251 cells. Rapamycin was used as an autophagy inducer. Scale bars = 20 μm.

(C) Western blotting analysis of the expression levels of TFR1 in NDV-infected U251cells. Western blotting samples corresponding to the marked timepoints were collected and analyzed.

(D and E) FTH1 and NCOA4 expression levels in NCOA4-knockdown cells. Cells were treated for 24 h with or without NDV. Data are representative of three experiments.

(F) Expression levels of Reactive oxygen species were observed in U251 cells with NCOA4 knockdown with fluorescence microscopy, Erastin was used as a ferroptosis inducer.

(J and H) Expression levels of ferrous iron in NCOA4-knockdown cells were observed with confocal fluorescence microscopy, Erastin was used as a ferroptosis inducer.

(I) Cell death was examined with an LDH assay 24 h after pretreatment with or without DFO.

(J) A model of the possible mechanisms underlying the induction of ferroptosis by NDV through nutrient deprivation and ferritinophagy in U251 cells.

Significance was analyzed using a two-tailed Student's t-test. *$p < 0.05$; **$p < 0.01$; ***$p < 0.001$. Data were expressed as mean ± SEM (n = 3 in each group).

iron is stored in ferritin, an iron storage protein complex consisting of FTH1 and FTL. Our results showed that FTH1 was shaped and decreased in a dose and time-dependent manner in NDV-infected U251 cells (Figures 2A–2D). Expression of FTH1 mRNA, detected using quantitative polymerase chain reaction, was consistent with protein levels (Figure 2E). Previous studies have shown that TFR1, a carrier protein for transferrin in cell membranes, is upregulated as ferroptosis proceeds. Our investigations showed that TFR1 was not upregulated in NDV-infected cells (Figure 4C).

To further investigate the important role of ferritinophagy in the process of ferroptosis, we knocked down the protein expression of NCOA4. Our results showed that the knockdown of NCOA4 significantly inhibited the reduction of FTH1 protein (Figures 4D and 4E). We also examined the expression level of lipid peroxides and ferrous iron after NCOA4 knockdown. Our findings indicated that NCOA4 deficiency suppressed the cellular levels of ROS and ferrous iron (Figures 4F–4H). To confirm that ferritinophagy promotes the initiation of ferroptosis, we knocked down the expression of autophagy-related gene 5 (ATG5), which caused the expression of ROS and Fe^{2+} to decrease significantly in NDV-infected cells (Figures S2B–2D). Deferoxamine (DFO), a membrane-impermeable iron chelator, is known to be a representative inhibitor of ferroptosis. Our results showed that cell death was rescued in DFO-treated NDV-infected cells (Figure 4I), and ROS levels were significantly reduced when NDV-infected cells were treated with DFO (Figures S2E and 2F). These results suggest that NDV accumulates ferrous iron via a decrease in ferritin through autophagy and induces ferroptosis in U251 cells.

DISCUSSION

Recent studies have shown that regulated cell death is an effective way to kill tumors. Triggering apoptosis cell death using anticancer drugs is a classical method of killing cancer cells (Badgley et al., 2020; Jiang et al., 2015; Sun et al., 2016; Tarangelo et al., 2018; Xie et al., 2017; Yang et al., 2014). However, the effects of apoptosis treatment of tumors are limited and the search for new therapies not relying on apoptosis to kill cancer cells will be important for treating therapy-resistant cancers in the future. Ferroptosis, a new form of programmed cell death, is typified by an iron-dependent accumulation of lethal levels of peroxidated lipids, and recent studies have suggested that ferroptosis is a tumor-suppressive mechanism(Stockwell et al., 2017; Yang et al., 2014). Our present study set out to understand the mechanisms of NDV-induced ferroptosis. We provide the evidence that different types of NDV strains induces ferroptosis through nutrient deprivation in U251 cells and that activation of p53 was responsible for suppressing system X_C^- and depleting the GSH contribution to lipid peroxidation. Our study suggested that the p53-SLC7A11-GPX4 axis plays a central role in inducing ferroptosis and leading to cancer cell death.

In this study, we showed that NDV suppressed system X_C^-, as evidenced by the decrease in SLC7A11 and SLC3A2 mRNA and protein levels in NDV-infected U251 cells. These results collectively suggest that NDV induces ferroptosis through nutrient deprivation in U251 cells. Consistent with our observations, Dixon et al. showed that System X_C^- is a cystine/glutamate antiporter whose activity suppresses ferroptosis in many different cell types (Dixon et al., 2012). Song et al. found that energy stress induces BECN1 activation and that BECN1 phosphorylation induces ferroptosis by blocking system X_C^- activity via binding to SLC7A11 (Song et al., 2018). In contrast, energy-stress-mediated AMPK activation inhibits ferroptosis via mediated phosphorylation of acetyl-CoA carboxylase and biosynthesis of PUFAs (Lee et al., 2020). Our results show that both SLC7A11 and SLC3A2 were suppressed in NDV-infected cells. Compared with previous studies, our study suggests that SLC3A2 plays an equally important role in the onset of ferroptosis by suppression of system X_C^- function. Recent studies have shown that system X_C^--mediated cystine import is necessary for GSH synthesis. The depletion of cystine, and/or GSH, results in the accumulation of lipid peroxidation products and lethal ROS in an iron-dependent manner (Stockwell et al., 2017).

The activation of p53, a tumor suppressor gene, has been implicated in contributing to the initiation of ferroptosis, and SLC7A11 was identified as a novel p53 target gene. p53 repression of SLC7A11 mRNA expression was observed in the tet-on p53-inducible line (Jiang et al., 2015). In contrast, MDM2 and MDMX induce ferroptosis independently of p53, although MDM2 and MDMX are negative regulators of p53 (Venkatesh et al., 2020). Wang et al. showed that acetylation is crucial for p53-mediated ferroptosis and identified a mouse p53 acetylation at K98 lysine (or at K101 for p53 in humans). The absence of acetylation resulted in the failure of p53 to mediate ferroptosis (Wang et al., 2016c). It has been reported that BRCA1-associated protein 1, another tumor suppressor, induces ferroptosis by repressing SLC7A11 in a similar way to p53 (Zhang et al., 2018). Our present study showed that p53 was upregulated in a dose- and time-dependent

manner in NDV-infected cells. Inhibition of p53 activation by specific p53 inhibitor, PFTα, blocked NDV-induced ferroptosis. Our results show that MDA production was reduced, and GSH was rescued, after PFTα blocked activation of p53 in NDV-infected cells. SLC7A11 protein and mRNA levels were also rescued after p53 was suppressed via siRNA. These results collectively suggest that p53 activation plays a critical role in inducing ferroptosis in NDV-infected cells.

As previously reported in the literature, TFR1 is a specific ferroptosis marker and the knockdown of TFR1 makes cells more resistant to erastin-induced cell death (Feng et al., 2020; Shen et al., 2018; Zhang et al., 2018, 2020). However, our study showed that the protein level of TFR1 was not upregulated in NDV-infected cells, while ferrous iron production and lipid peroxidation were upregulated after NDV infection in U251 cells (Figure 4C). All the results shown above are characteristic of ferroptosis. This is an unresolved issue that requires further investigation of the differences between chemical molecular and virus-induced ferroptosis. Ferrous iron accumulation via ferritin decreases in cells induced Fenton mediation and boosted ROS accumulation to cause lipid peroxidation and to enhance ferroptosis (Liu et al., 2020; Zhou et al., 2020). Accumulating evidence suggests that lysosomes can accumulation iron through degradation of FTH1. NCOA4 has been identified as a cargo receptor (known as ferritinophagy) and recruits FTH1 to autophagosomes, while iron release induces ferroptosis (Gao et al., 2016; Hou et al., 2016). Our previous studies showed that NDV triggers autophagy and promotes virus replication in U251 glioma cells (Meng et al., 2012). Here, we have shown that NCOA4 and FTH1 are significantly reduced by autophagy in NDV-infected cells. Hou et al. showed that autophagy induces ferroptosis through the degradation of ferritin (Hou et al., 2016). Consistent with their studies, our results suggest that intercellular ferritin levels were decreased by lysosomes through autophagy enhanced ferroptosis in NDV-infected cells. When ferritinophagy was inhibited by the knockdown of NCOA4, the increases in lipid peroxidation and ferrous iron were both inhibited, which is in consistent with previous findings ((Hou et al., 2016)).

Recent studies have shown that ferroptotic responses are often dependent on acyl-CoA synthetase long-chain family member 4. ACSL4 catalyzes the incorporation of PUFAs into membrane phospholipids and enhances ferroptosis (Doll et al., 2017). Li et al. documented that zalcitabine induces ALOX5-dependent ferroptosis in pancreatic cancer cells, but not ALOX12. Zalcitabine treatment failed to reduce the size of tumors formed and upregulated ACSL4 expression in ALOX5 and ATG5 knockdown PANC1 cell lines (Li et al., 2021). However, Chu et al. showed that ferroptosis can occur in an ACSL4-independent manner and that ALOX12 is required for p53-mediated tumor suppression through ferroptosis (Chu et al., 2019). Consistent with this, our results show that ALOX12 is upregulated by NDV infection and ACSL4 activation is not necessary for NDV-induced ferroptosis (Figure S2G). Recent findings report AMPK-mediated beclin-1 phosphorylation induces ferroptosis (Matthew-Onabanjo et al., 2020; Song et al., 2018). However, Lee et al. showed that PUFAs can be synthesized from the basic building block acetyl coenzyme A carboxylase and that AMPK suppresses ferroptosis by inhibiting ACC (Lee et al., 2020). These results suggest that NDV-induced ferroptosis is an ACSL4-independent pathway. Our present study showed that lipid peroxidation accumulation, as tested using fluorescence probes, and cell death can be suppressed by liproxstain-1 and deferoxamine (Figures 1J and 4I). Our findings were limited to the clarification of the mechanism of lipid peroxidation increase in ACSL4-independent manner. Further study is needed to better understand the details of this phenomenon.

In summary, our study demonstrated (1) that NDV-induced ferroptosis acts through nutrient deprivation by suppression of system X_C^-; (2) that p53 activation is required for ferroptosis initiation; and (3) that the ferritinophagy induced by NDV promotes ferroptosis through the release of ferrous iron. Our study first reported that NDV-induced ferroptosis acts via nutrient deprivation and that oncolytic virus can kill cancer cells through ferroptosis. Our results explain how NDV infection induces ferroptosis and provide novel insights into new treatments for therapy-resistant cancers.

Limitations of the study

The mechanisms of NDV-induced ferroptosis still need to be elucidated. Our previous reports identified two types of cell death, apoptosis, and pyroptosis, but not necroptosis, induced by NDV infection (Li et al., 2019; Wang et al., 2016b; Ying et al., 2017), indicating that NDV-induced cell death types were diverse. Therefore, which type of cell death is dominant in the process of NDV-induced tumor cell death should be investigated further. In addition, although our study has experimentally demonstrated the mechanisms of NDV-induced ferroptosis in cultured cells, the role of ferroptosis caused by NDV in killing tumor cells requires further validation in animal models.

STAR★METHODS

Detailed methods are provided in the online version of this paper and include the following:

- KEY RESOURCES TABLE
- RESOURCE AVAILABILITY
  - Lead contact
  - Materials availability
  - Data and code availability
- EXPERIMENTAL MODEL AND SUBJECT DETAILS
- METHOD DETAILS
  - Living cell image analysis
  - Cell viability assay
  - siRNA transfection and flow cytometry
  - Western blotting
  - RNA isolation and quantitative real-time PCR (qRT–PCR)
  - Lipid peroxidation assay and MDA assay
  - GSH/GSHG assay
- QUANTIFICATION AND STATISTICAL ANALYSIS

SUPPLEMENTAL INFORMATION

Supplemental information can be found online at https://doi.org/10.1016/j.isci.2021.102837.

ACKNOWLEDGMENTS

This work was funded by National Natural Science Foundation of China (No.32030108).

AUTHOR CONTRIBUTIONS

Chan Ding and Yingjie Sun conceived of and designed the experiments. Xianjin Kan and Yuncong Yin performed the experiments and analyzed the data. Xianjin Kan prepared the figures and wrote the manuscript. Cuiping Song, Lei Tan, Xusheng Qiu, Ying Liao, Weiwei Liu, Songshu Meng contributed reagents, materials, analysis tools, and discussions. Chan Ding and Yingjie Sun revised the manuscript. All authors read and approved the final manuscript.

DECLARATION OF INTERESTS

The authors declare that they have no competing interests.

INCLUSION AND DIVERSITY

We worked to ensure diversity in experimental samples through the selection of the cell lines. We worked to ensure diversity in experimental samples through the selection of the genomic datasets. While citing references scientifically relevant for this work, we also actively worked to promote gender balance in our reference list.

Received: December 30, 2020
Revised: May 31, 2021
Accepted: July 7, 2021
Published: August 20, 2021

REFERENCES

Ajoolabady, A., Aslkhodapasandhokmabad, H., Libby, P., Tuomilehto, J., Lip, G.Y.H., Penninger, J.M., Richardson, D.R., Tang, D., Zhou, H., Wang, S., et al. (2021). Ferritinophagy and ferroptosis in the management of metabolic diseases. Trends Endocrinol. Metab. https://doi.org/10.1016/j.tem.2021.04.010.

Alborzinia, H., Ignashkova, T.I., Dejure, F.R., Gendarme, M., Theobald, J., Wolfl, S., Lindemann, R.K., and Reiling, J.H. (2018). Golgi stress mediates redox imbalance and ferroptosis in human cells. Commun. Biol. *1*, 210. https://doi.org/10.1038/s42003-018-0212-6.

Alexander, D.J. (2000). Newcastle disease and other avian paramyxoviruses. Rev. Sci. Tech. *19*, 443–462.

Anandhan, A., Dodson, M., Schmidlin, C.J., Liu, P., and Zhang, D.D. (2020). Breakdown of an ironclad defense system: the critical role of NRF2 in mediating ferroptosis. Cell Chem Biol. *27*, 436–447. https://doi.org/10.1016/j.chembiol.2020.03.011.

Angeli, J.P.F., Shah, R., Pratt, D.A., and Conrad, M. (2017). Ferroptosis inhibition: mechanisms and opportunities. Trends Pharmacol. Sci. *38*, 489–498. https://doi.org/10.1016/j.tips.2017.02.005.

Badgley, M.A., Kremer, D.M., Maurer, H.C., DelGiorno, K.E., Lee, H.J., Purohit, V., Sagalovskiy, I.R., Ma, A., Kapilian, J., Firl, C.E.M., et al. (2020). Cysteine depletion induces pancreatic tumor ferroptosis in mice. Science *368*, 85–89. https://doi.org/10.1126/science.aaw9872.

Bersuker, K., Hendricks, J.M., Li, Z., Magtanong, L., Ford, B., Tang, P.H., Roberts, M.A., Tong, B., Maimone, T.J., Zoncu, R., et al. (2019). The CoQ oxidoreductase FSP1 acts parallel to GPX4 to inhibit ferroptosis. Nature *575*, 688–692. https://doi.org/10.1038/s41586-019-1705-2.

Cao, J.Y., and Dixon, S.J. (2016). Mechanisms of ferroptosis. Cell Mol. Life Sci. *73*, 2195–2209. https://doi.org/10.1007/s00018-016-2194-1.

Chu, B., Kon, N., Chen, D., Li, T., Liu, T., Jiang, L., Song, S., Tavana, O., and Gu, W. (2019). ALOX12 is required for p53-mediated tumour suppression through a distinct ferroptosis pathway. Nat. Cell Biol. *21*, 579–591. https://doi.org/10.1038/s41556-019-0305-6.

Colunga, A.G., Laing, J.M., and Aurelian, L. (2010). The HSV-2 mutant DeltaPK induces melanoma oncolysis through nonredundant death programs and associated with autophagy and pyroptosis proteins. Gene Ther. *17*, 315–327. https://doi.org/10.1038/gt.2009.126.

Dixon, S.J., Lemberg, K.M., Lamprecht, M.R., Skouta, R., Zaitsev, E.M., Gleason, C.E., Patel, D.N., Bauer, A.J., Cantley, A.M., Yang, W.S., et al. (2012). Ferroptosis: an iron-dependent form of nonapoptotic cell death. Cell *149*, 1060–1072. https://doi.org/10.1016/j.cell.2012.03.042.

Dixon, S.J., and Stockwell, B.R. (2014). The role of iron and reactive oxygen species in cell death. Nat. Chem. Biol. *10*, 9–17. https://doi.org/10.1038/nchembio.1416.

Doll, S., Freitas, F.P., Shah, R., Aldrovandi, M., da Silva, M.C., Ingold, I., Goya Grocin, A., Xavier da Silva, T.N., Panzilius, E., Scheel, C.H., et al. (2019). FSP1 is a glutathione-independent ferroptosis suppressor. Nature *575*, 693–698. https://doi.org/10.1038/s41586-019-1707-0.

Doll, S., Proneth, B., Tyurina, Y.Y., Panzilius, E., Kobayashi, S., Ingold, I., Irmler, M., Beckers, J., Aichler, M., Walch, A., et al. (2017). ACSL4 dictates ferroptosis sensitivity by shaping cellular lipid composition. Nat. Chem. Biol. *13*, 91–98. https://doi.org/10.1038/nchembio.2239.

Fang, X., Cai, Z., Wang, H., Han, D., Cheng, Q., Zhang, P., Gao, F., Yu, Y., Song, Z., Wu, Q., et al. (2020). Loss of cardiac ferritin H facilitates cardiomyopathy via Slc7a11-mediated ferroptosis. Circ. Res. *127*, 486–501. https://doi.org/10.1161/CIRCRESAHA.120.316509.

Feng, H., Schorpp, K., Jin, J., Yozwiak, C.E., Hoffstrom, B.G., Decker, A.M., Rajbhandari, P., Stokes, M.E., Bender, H.G., Csuka, J.M., et al. (2020). Transferrin receptor is a specific ferroptosis marker. Cell Rep. *30*, 3411–3423.e7. https://doi.org/10.1016/j.celrep.2020.02.049.

Fiola, C., Peeters, B., Fournier, P., Arnold, A., Bucur, M., and Schirrmacher, V. (2006). Tumor selective replication of Newcastle disease virus: association with defects of tumor cells in antiviral defence. Int. J. Cancer *119*, 328–338. https://doi.org/10.1002/ijc.21821.

Gao, M., Monian, P., Pan, Q., Zhang, W., Xiang, J., and Jiang, X. (2016). Ferroptosis is an autophagic cell death process. Cell Res. *26*, 1021–1032. https://doi.org/10.1038/cr.2016.95.

Gao, M., Yi, J., Zhu, J., Minikes, A.M., Monian, P., Thompson, C.B., and Jiang, X. (2019). Role of mitochondria in ferroptosis. Mol. Cell *73*, 354–363.e3. https://doi.org/10.1016/j.molcel.2018.10.042.

Goodall, M., and Thorburn, A. (2014). Identifying specific receptors for cargo-mediated autophagy. Cell Res. *24*, 783–784. https://doi.org/10.1038/cr.2014.56.

Hadian, K., and Stockwell, B.R. (2020). SnapShot: ferroptosis. Cell *181*, 1188–1188.e1. https://doi.org/10.1016/j.cell.2020.04.039.

Hassannia, B., Vandenabeele, P., and Vanden Berghe, T. (2019). Targeting ferroptosis to iron out cancer. Cancer Cell *35*, 830–849. https://doi.org/10.1016/j.ccell.2019.04.002.

Hou, W., Xie, Y., Song, X., Sun, X., Lotze, M.T., Zeh, H.J., 3rd, Kang, R., and Tang, D. (2016). Autophagy promotes ferroptosis by degradation of ferritin. Autophagy *12*, 1425–1428. https://doi.org/10.1080/15548627.2016.1187366.

Ito, J., Omiya, S., Rusu, M.C., Ueda, H., Murakawa, T., Tanada, Y., Abe, H., Nakahara, K., Asahi, M., Taneike, M., et al. (2021). Iron derived from autophagy-mediated ferritin degradation induces cardiomyocyte death and heart failure in mice. Elife *10*. https://doi.org/10.7554/eLife.62174.

Jiang, L., Kon, N., Li, T., Wang, S.J., Su, T., Hibshoosh, H., Baer, R., and Gu, W. (2015). Ferroptosis as a p53-mediated activity during tumour suppression. Nature *520*, 57–62. https://doi.org/10.1038/nature14344.

Koks, C.A., Garg, A.D., Ehrhardt, M., Riva, M., Vandenberk, L., Boon, L., De Vleeschouwer, S., Agostinis, P., Graf, N., and Van Gool, S.W. (2015). Newcastle disease virotherapy induces long-term survival and tumor-specific immune memory in orthotopic glioma through the induction of immunogenic cell death. Int. J. Cancer *136*, E313–E325. https://doi.org/10.1002/ijc.29202.

Lee, H., Zandkarimi, F., Zhang, Y., Meena, J.K., Kim, J., Zhuang, L., Tyagi, S., Ma, L., Westbrook, T.F., Steinberg, G.R., et al. (2020). Energy-stress-mediated AMPK activation inhibits ferroptosis. Nat. Cell Biol. *22*, 225–234. https://doi.org/10.1038/s41556-020-0461-8.

Li, C., Zhang, Y., Liu, J., Kang, R., Klionsky, D.J., and Tang, D. (2021). Mitochondrial DNA stress triggers autophagy-dependent ferroptotic death. Autophagy *17*, 948–960. https://doi.org/10.1080/15548627.2020.1739447.

Li, Y., Jiang, W., Niu, Q., Sun, Y., Meng, C., Tan, L., Song, C., Qiu, X., Liao, Y., and Ding, C. (2019). eIF2alpha-CHOP-BCl-2/JNK and IRE1alpha-XBP1/JNK signaling promote apoptosis and inflammation and support the proliferation of Newcastle disease virus. Cell Death Dis. *10*, 891. https://doi.org/10.1038/s41419-019-2128-6.

Liu, J., Kuang, F., Kroemer, G., Klionsky, D.J., Kang, R., and Tang, D. (2020). Autophagy-dependent ferroptosis: machinery and regulation. Cell Chem. Biol. *27*, 420–435. https://doi.org/10.1016/j.chembiol.2020.02.005.

Lv, H., Zhen, C., Liu, J., Yang, P., Hu, L., and Shang, P. (2019). Unraveling the potential role of glutathione in multiple forms of cell death in cancer therapy. Oxid Med. Cell Longev. *2019*, 3150145. https://doi.org/10.1155/2019/3150145.

Mansour, M., Palese, P., and Zamarin, D. (2011). Oncolytic specificity of Newcastle disease virus is mediated by selectivity for apoptosis-resistant cells. J. Virol. *85*, 6015–6023. https://doi.org/10.1128/JVI.01537-10.

Masaldan, S., Clatworthy, S.A.S., Gamell, C., Meggyesy, P.M., Rigopoulos, A.T., Haupt, S., Haupt, Y., Denoyer, D., Adlard, P.A., Bush, A.I., and Cater, M.A. (2018). Iron accumulation in senescent cells is coupled with impaired ferritinophagy and inhibition of ferroptosis. Redox Biol. *14*, 100–115. https://doi.org/10.1016/j.redox.2017.08.015.

Matthew-Onabanjo, A.N., Janusis, J., Mercado-Matos, J., Carlisle, A.E., Kim, D., Levine, F., Cruz-Gordillo, P., Richards, R., Lee, M.J., and Shaw, L.M. (2020). Beclin 1 promotes endosome recruitment of hepatocyte growth factor tyrosine kinase Substrate to suppress tumor proliferation. Cancer Res. *80*, 249–262. https://doi.org/10.1158/0008-5472.CAN-19-1555.

Meng, C., Zhou, Z., Jiang, K., Yu, S., Jia, L., Wu, Y., Liu, Y., Meng, S., and Ding, C. (2012). Newcastle disease virus triggers autophagy in U251 glioma cells to enhance virus replication. Arch. Virol. *157*, 1011–1018. https://doi.org/10.1007/s00705-012-1270-6.

Muri, J., Thut, H., Bornkamm, G.W., and Kopf, M. (2019). B1 and marginal zone B cells but not follicular B2 cells require Gpx4 to prevent lipid peroxidation and ferroptosis. Cell Rep. *29*, 2731–2744.e4. https://doi.org/10.1016/j.celrep.2019.10.070.

Nai, A., Lidonnici, M.R., Federico, G., Pettinato, M., Olivari, V., Carrillo, F., Geninatti Crich, S., Ferrari, G., Camaschella, C., Silvestri, L., and Carlomagno, F. (2021). NCOA4-mediated ferritinophagy in macrophages is crucial to sustain erythropoiesis in mice. Haematologica *106*, 795–805. https://doi.org/10.3324/haematol.2019.241232.

Qin, X., Zhang, J., Wang, B., Xu, G., Yang, X., Zou, Z., and Yu, C. (2021). Ferritinophagy is involved in the zinc oxide nanoparticles-induced ferroptosis of vascular endothelial cells. Autophagy *1*, 20. https://doi.org/10.1080/15548627.2021.1911016.

Ren, S., Ur Rehman, Z., Gao, B., Yang, Z., Zhou, J., Meng, C., Song, C., Nair, V., Sun, Y., and Ding, C. (2020). ATM-mediated DNA double-strand break response facilitated oncolytic Newcastle disease virus replication and promoted syncytium formation in tumor cells. PLoS Pathog. *16*, e1008514. https://doi.org/10.1371/journal.ppat.1008514.

Shen, Y., Li, X., Dong, D., Zhang, B., Xue, Y., and Shang, P. (2018). Transferrin receptor 1 in cancer: a new sight for cancer therapy. Am. J. Cancer Res. *8*, 916–931.

Song, X., Zhu, S., Chen, P., Hou, W., Wen, Q., Liu, J., Xie, Y., Liu, J., Klionsky, D.J., Kroemer, G., et al. (2018). AMPK-mediated BECN1 phosphorylation

promotes ferroptosis by directly blocking system Xc(-) activity. Curr. Biol. *28*, 2388–2399.e5. https://doi.org/10.1016/j.cub.2018.05.094.

Stockwell, B.R., Friedmann Angeli, J.P., Bayir, H., Bush, A.I., Conrad, M., Dixon, S.J., Fulda, S., Gascon, S., Hatzios, S.K., Kagan, V.E., et al. (2017). Ferroptosis: a regulated cell death Nexus linking metabolism, redox biology, and disease. Cell *171*, 273–285. https://doi.org/10.1016/j.cell.2017.09.021.

Su, L.J., Zhang, J.H., Gomez, H., Murugan, R., Hong, X., Xu, D., Jiang, F., and Peng, Z.Y. (2019). Reactive oxygen species-induced lipid peroxidation in apoptosis, autophagy, and ferroptosis. Oxid. Med. Cell Longev. *2019*, 5080843. https://doi.org/10.1155/2019/5080843.

Sun, X., Ou, Z., Chen, R., Niu, X., Chen, D., Kang, R., and Tang, D. (2016). Activation of the p62-Keap1-NRF2 pathway protects against ferroptosis in hepatocellular carcinoma cells. Hepatology *63*, 173–184. https://doi.org/10.1002/hep.28251.

Tang, D., Chen, X., Kang, R., and Kroemer, G. (2021). Ferroptosis: molecular mechanisms and health implications. Cell Res. *31*, 107–125. https://doi.org/10.1038/s41422-020-00441-1.

Tarangelo, A., Magtanong, L., Bieging-Rolett, K.T., Li, Y., Ye, J., Attardi, L.D., and Dixon, S.J. (2018). p53 suppresses metabolic stress-induced ferroptosis in cancer cells. Cell Rep. *22*, 569–575. https://doi.org/10.1016/j.celrep.2017.12.077.

Ubellacker, J.M., Tasdogan, A., Ramesh, V., Shen, B., Mitchell, E.C., Martin-Sandoval, M.S., Gu, Z., McCormick, M.L., Durham, A.B., Spitz, D.R., et al. (2020). Lymph protects metastasizing melanoma cells from ferroptosis. Nature *585*, 113–118. https://doi.org/10.1038/s41586-020-2623-z.

Venkatesh, D., O'Brien, N.A., Zandkarimi, F., Tong, D.R., Stokes, M.E., Dunn, D.E., Kengmana, E.S., Aron, A.T., Klein, A.M., Csuka, J.M., et al. (2020). MDM2 and MDMX promote ferroptosis by PPARalpha-mediated lipid remodeling. Genes Dev. *34*, 526–543. https://doi.org/10.1101/gad.334219.119.

Wang, B., Zhang, J., Song, F., Tian, M., Shi, B., Jiang, H., Xu, W., Wang, H., Zhou, M., Pan, X., et al. (2016a). EGFR regulates iron homeostasis to promote cancer growth through redistribution of transferrin receptor 1. Cancer Lett. *381*, 331–340. https://doi.org/10.1016/j.canlet.2016.08.006.

Wang, B., Zhu, J., Li, D., Wang, Y., Zhan, Y., Tan, L., Qiu, X., Sun, Y., Song, C., Meng, C., et al. (2016b). Newcastle disease virus infection induces activation of the NLRP3 inflammasome. Virology *496*, 90–96. https://doi.org/10.1016/j.virol.2016.05.023.

Wang, S.J., Li, D., Ou, Y., Jiang, L., Chen, Y., Zhao, Y., and Gu, W. (2016c). Acetylation is crucial for p53-mediated ferroptosis and tumor suppression. Cell Rep. *17*, 366–373. https://doi.org/10.1016/j.celrep.2016.09.022.

Xie, Y., Hou, W., Song, X., Yu, Y., Huang, J., Sun, X., Kang, R., and Tang, D. (2016). Ferroptosis: process and function. Cell Death Differ. *23*, 369–379. https://doi.org/10.1038/cdd.2015.158.

Xie, Y., Zhu, S., Song, X., Sun, X., Fan, Y., Liu, J., Zhong, M., Yuan, H., Zhang, L., Billiar, T.R., et al. (2017). The tumor suppressor p53 limits ferroptosis by blocking DPP4 activity. Cell Rep. *20*, 1692–1704. https://doi.org/10.1016/j.celrep.2017.07.055.

Yang, W.S., SriRamaratnam, R., Welsch, M.E., Shimada, K., Skouta, R., Viswanathan, V.S., Cheah, J.H., Clemons, P.A., Shamji, A.F., Clish, C.B., et al. (2014). Regulation of ferroptotic cancer cell death by GPX4. Cell *156*, 317–331. https://doi.org/10.1016/j.cell.2013.12.010.

Yang, W.S., and Stockwell, B.R. (2016). Ferroptosis: death by lipid peroxidation. Trends Cell Biol. *26*, 165–176. https://doi.org/10.1016/j.tcb.2015.10.014.

Ying, L., Xiang, M., Meng, G., and Ding, C. (2017). RIP1 is a central signaling protein in regulation of TNF-α:TRAIL mediated apoptosis and necroptosis during Newcastle disease virus infection.pdf. Oncotarget *8*, 43201–43217.

Yu, D., Liu, Y., Zhou, Y., Ruiz-Rodado, V., Larion, M., Xu, G., and Yang, C. (2020). Triptolide suppresses IDH1-mutated malignancy via Nrf2-driven glutathione metabolism. Proc. Natl. Acad. Sci. U S A *117*, 9964–9972. https://doi.org/10.1073/pnas.1913633117.

Zhang, S., Cao, Y., and Yang, Q. (2020). Transferrin receptor 1 levels at the cell surface influence the susceptibility of newborn piglets to PEDV infection. PLoS Pathog. *16*, e1008682. https://doi.org/10.1371/journal.ppat.1008682.

Zhang, Y., Shi, J., Liu, X., Feng, L., Gong, Z., Koppula, P., Sirohi, K., Li, X., Wei, Y., Lee, H., et al. (2018). BAP1 links metabolic regulation of ferroptosis to tumour suppression. Nat. Cell Biol. *20*, 1181–1192. https://doi.org/10.1038/s41556-018-0178-0.

Zhou, B., Liu, J., Kang, R., Klionsky, D.J., Kroemer, G., and Tang, D. (2020). Ferroptosis is a type of autophagy-dependent cell death. Semin. Cancer Biol. *66*, 89–100. https://doi.org/10.1016/j.semcancer.2019.03.002.

STAR★METHODS

KEY RESOURCES TABLE

REAGENT or RESOURCE	SOURCE	IDENTIFIER
Antibodies		
Mouse monoclonal anti-β-actin	Santa Cruz Biotechnology	Cat# sc-8432, RRID:AB_626630
Mouse monoclonal anti-ACSL4	Santa Cruz Biotechnology	Cat# sc-271800, RRID:AB_10715092
Mouse monoclonal anti-NP	Prepared in our laboratory.	N/A
Mouse monoclonal anti-p53	Abcam	Cat# ab26, RRID:AB_303198
Rabbit monoclonal anti-SLC7A11	Abcam	Cat# ab175186, RRID:AB_2722749
Rabbit monoclonal anti-GPX4	Abcam	Cat# ab125066, RRID:AB_10973901
Rabbit polyclonal anti-ALOX12	Abcam	Cat# ab211506
Rabbit polyclonal anti-NCOA4	Abcam	Cat# ab86707, RRID:AB_1925236
Rabbit monoclonal ant-FTH1	Cell Signaling Technology	Cat# 4393, RRID:AB_11217441
Rabbit monoclonal ant-TFR1	Cell Signaling Technology	Cat# 13208, RRID:AB_2798150
Rabbit monoclonal ant-SLC3A2	Cell Signaling Technology	Cat# 47213, RRID:AB_2799323
Rabbit monoclonal ant-LC3B	Cell Signaling Technology	Cat# 3868, RRID:AB_2137707
Bacterial and virus strains		
NDV strain Herts/33	China Institute of Veterinary Drug Control (Beijing, China)	N/A
NDV strain ZJ1	Provided by Shunlin Hu (Yangzhou University, Yangzhou, China)	N/A
Ubi-senseGFP-LC3-SV40-pur	Shanghai Genechem Co., Ltd	N/A
Chemicals, peptides, and recombinant proteins		
RSL3	Selleck	S8155; CAS: 1219810-16-8
Erastin	Selleck	S7242; CAS: 571203-78-6
Liproxstatin-1(Lip-1)	Selleck	S7699; CAS: 950455-15-9
Bafilomycin (Baf-A1)	Selleck	S1413; CAS: 88899-55-2
Pifithrin-α (PFTα) HBr	Selleck	S2929; CAS: 63208-82-2
Dimethyl sulfoxide (DMSO)	Sigma	Cat# D2650
FuGEN HD	Promega	Cat# E2311
OPTI-MEM ® medium	Gibco	Cat# 11965500BT
Deferoxamine mesylate (DFO)	Selleck	S5742; CAS: 138-14-7
Critical commercial assays		
Pierce BCA protein Assay Kit	Thermo Fisher	23225
Halt™ Protease and Phosphatase Inhibitor Single-Use Cocktail (100X)	Thermo Fisher	78442
GSSG/GSH quantification kits II	DoJindo	G263
Lipid Peroxidation (MDA) Assay Kit	Beyotime	S0131M
Hoechst 33342	Beyotime	C1022
DCFDA/H2DCFDA	Abacm	ab113851
Cell Counting Kit-8	DoJindo	CK04
Cytotoxicity LDH Assay Kit-WST	DoJindo	CK12

(*Continued on next page*)

Continued

REAGENT or RESOURCE	SOURCE	IDENTIFIER
FerroOrange	DoJindo	F374
SYBR Green qPCR Mix	GDSBio	P2092
Liperfluo	DoJindo	L248
Experimental models: Cell lines		
Human glioma cells U251	Cell Bank of the Shanghai Institute of Biochemistry and Cell Biology	TCHu58
U251-GFP-LC3	This paper	N/A
Oligonucleotides		
qPCR primers for mRNA validation, see Table S1	This paper	N/A
Primer for siRNA validation, see Table S2	This paper	N/A
Software and algorithms		
Image J	NIH	https://imagej.nih.gov/ij/
GraphPad prism	GraphPad Software	https://www.graphpad.com/
FlowJo	FlowJo	https://www.flowjo.com/

RESOURCE AVAILABILITY

Lead contact

Further information and requests for resources and reagents should be directed to and will be fulfilled by the lead contact, Chan Ding (shoveldeen@shvri.ac.cn).

Materials availability

This study did not generate new unique reagents.

Data and code availability

Original data for figures in the paper are available at Mendeley Data: https://doi.org/10.17632/r27s7f2yyh.1#file-b17cefad-24b8-43ff-b472-02b576e5aa49

EXPERIMENTAL MODEL AND SUBJECT DETAILS

Human glioma cells U251 were purchased from the Cell Bank of the Shanghai Institute of Biochemistry and Cell Biology, Chinese Academy of Science (Shanghai, China) (http://www.cellbank.org.cn). U251 cells were cultured in Dulbecco's Modified Eagle Medium (DMEM) supplemented with 10% fetal bovine serum, 100 μg ml $^{-1}$penicillin, and 100 μg ml $^{-1}$streptomycin (Thermo Fisher Scientific, Waltham, MA, USA). Cells were cultured at 37°C in an incubator with 5% CO_2. A stable GFP-LC3 cell line was generated by infecting U251 cells with a lentiviral vector encoding an GFP-LC3 reporter, and human glioma U251 cells (1×10^6–2×10^6 cells) were prepared and infected at a multiplicity of infection (MOI) of 10, with GFP-LC3-overexpressing lentiviruses (GeneChem, Shanghai, China).

METHOD DETAILS

Living cell image analysis

U251 cells were seeded into six-well plates and incubated for 24 h before the experiment began. Inducers or inhibitors were infected with NDV and co-incubated for 24 h. Cells were washed with PBS and then stained with Hoechst 33342 for 10 min at 37°C in the dark, and then washed extensively with PBS. U251 cells were incubated with FerroOrange following the manufacturer's instructions. Finally, ferrous iron imaging of the living cells was performed using a fluorescence microscope.

Cell viability assay

For the cell viability assay, the cells were seeded at 50,000 cells per well in 96-well plates. At 24 h after seeding, the cells were treated with the indicated concentrations of Erastin, RSL3, and NDV, in accordance with the manufacturer's guidelines. The Cytotoxicity LDH Assay Kit-WST® were purchased from Dojindo Molecular Technologies, Inc. (Shanghai, China).

siRNA transfection and flow cytometry

For experimental transfection, cells were cultured to approximately 50%–60% confluence in six-well plates and transfected with 1 μg of siRNA (siRNA NC, siRNA p53, siRNA NCOA4, or siRNA ATG5) using FuGENE HD (Promega, Madison, WI, USA), in accordance with the manufacturer's guidelines. The cells were incubated at 37 °C with 5% CO_2 for 5 h and cultured in DMEM supplemented with 2% FBS for further experiments. At 48 h after siRNA transfection, the efficiency of knockdown was determined with western blotting. The siRNAs used in this study were synthesized by GenePharma (Shanghai, China). For flow cytometry, cells (1×10^6 cells/well) were plated in a six-well plate and maintained overnight. The cells were then incubated with drugs and NDV for the appropriate time. The cells were washed twice and suspended in 400 μl of DCFH-DA working solution at 37 °C for 30 min. After the cells were washed with PBS, the intracellular ROS production was evaluated with a flow cytometer at an excitation wavelength of 485 nm. For each sample, approximately 10,000 cells were assessed. All assays were performed as three replicates.

Western blotting

U251 cells were seeded into six-well plates, infected with NDV (MOI 5), and incubated for 12, 24, and 36 h, or incubated for 24 h in either the presence or absence of inhibitors. Cell samples were washed with PBS and lysed in NP-40 lysis buffer (50 mM Tris-HCl, pH 8.0, 5 mm EGTA, 150 mM NaCl, 2 mM sodium vanadate, 5 mM EDTA, 1% NP-40, and 1 mM NaF) with a cocktail of protease inhibitors (Pierce Chemical, Rockford, IL, USA). Cell lysates were prepared and analyzed for the expression of the indicated proteins using their specific antibodies, followed by treatment with horseradish peroxidase-conjugated secondary antibodies IgG using a chemiluminescence reagent solution kit (Share-bio-Biotechnology, Shanghai, China). β-actin was used as a loading control.

RNA isolation and quantitative real-time PCR (qRT–PCR)

U251 cells were seeded into six-well plates and total RNA was extracted using TRIzol ® Reagent (Invitrogen, USA) according to the manufacturer's instructions. cDNA was reverse transcribed from total RNA using expand reverse transcriptase (Roche, USA) and oligo-dT primer. For the quantitative RT–PCR analysis, the mRNA levels of specific genes were calculated using β-actin as the reference gene. The experiment was performed in triplicate and the mean result determined.

Lipid peroxidation assay and MDA assay

The lipid peroxidation was determined using Liperfluo (Green), and the detection of MDA concentration in cell lysates was performed strictly to the manufacturer's instructions (Beyotime, China). Liperfluo, a Spy-LHP analog, is used for lipid peroxide detection and emits intense fluorescence due to lipid peroxide-specific oxidation which allows lipid peroxide imaging using a fluorescence microscope to view living cells. For MDA detection, the thiobarbituric acid included in the kit was added to the supernatants of cell homogenate to form a TBA-MDA mixture, which was then examined spectrophotometrically at 535 nm. All assays were performed with three independent replications.

GSH/GSHG assay

The intracellular levels of reductive GSH were determined using a GSSG/GSH quantification kit, to detect reductive GSH concentrations in cell lysates, strictly according to the manufacturer's instructions. The absorbance was measured at 405 nm or 415 nm. The experiment was performed as three independent replicates.

QUANTIFICATION AND STATISTICAL ANALYSIS

Statistical analyses were performed using GraphPad Prism 8 software (Graph Pad Software, Inc., San Diego, CA, USA). The data were expressed as means ± standard deviation (SD) of at least three independent replications. analyzed using an unpaired Student's t-test. A p value of < 0.05 was considered statistically significant. ns, $p > 0.05$; *$p < 0.05$; **$p < 0.01$, ***$p < 0.001$.